Microphysical transition in water clouds over the Amazon and China derived from space-borne radar and radiometer data

Kazuaki Kawamoto[1] and Kentaroh Suzuki[2,3]

Received 15 June 2011; revised 23 January 2012; accepted 23 January 2012; published 14 March 2012.

[1] This study examines the transitional processes and relationships among cloud droplets, drizzle, and precipitation in single-layer water clouds over the Amazon and China by synergistically analyzing products of active CloudSat and passive Moderate Resolution Imaging Spectroradiometer sensors. Cloud droplet number concentrations (N_c) are confirmed to generally be lower over the Amazon and higher over China, reflecting the difference in aerosol amount between these two regions at different seasons. Radar reflectivity (Z_e) frequencies are consistent with the regional and seasonal differences in precipitation rate. Furthermore, the fractional occurrences of maximum Z_e as a function of liquid water path (LWP) show an almost monotonic decline and increase for nonprecipitating and precipitating categories, respectively, denoting differences in the precipitation rate. The behavior of cloud parameters such as the cloud optical depth, effective particle radius, N_c, and LWP among different Z_e categories indicates the cloud development stage and reveals regional differences in the microphysical characteristics. Finally, a vertical cloud structure is examined to illustrate that water clouds tend to become optically thinner and to produce precipitation (shifting to larger Z_e) through the coalescence of droplets as N_c decreases. Regionally, precipitation over the Amazon takes place in optically thicker parts than over China.

Citation: Kawamoto, K., and K. Suzuki (2012), Microphysical transition in water clouds over the Amazon and China derived from space-borne radar and radiometer data, *J. Geophys. Res.*, *117*, D05212, doi:10.1029/2011JD016412.

1. Introduction

[2] Clouds play key roles in climate systems; for example, they produce precipitation and control the global energy budget via their effects on solar and infrared radiative transfer processes. It is important to understand cloud vertical structure and microphysical properties such as optical depth (τ_c) and effective particle radius (r_e) for determining the effects of clouds on climate [e.g., *Stephens et al.*, 2008].

[3] Water clouds occupy a large area of the atmosphere over both oceans and land and have been investigated more extensively than ice clouds for several reasons. One reason is that in situ measurements are easier to conduct for water clouds, which occur in the lower atmosphere, than for high-altitude ice clouds. Moreover, because water droplets are assumed to be spherical, Mie scattering theory can be applied to radiative transfer calculations. Conversely, it is difficult to determine the scattering properties of the nonspherical particles found in ice clouds.

[4] Remote sensing of visible and infrared wavelengths by passive sensors has been achieved using the Advanced Very High Resolution Radiometer (AVHRR) [e.g., *Han et al.*, 1994; *Kawamoto et al.*, 2001] and Moderate Resolution Imaging Spectroradiometer (MODIS) [e.g., *Platnick et al.*, 2003]. Recently, active remote sensing has also become available, such as from the CloudSat satellite. Launched in April 2006, CloudSat carries the Cloud Profiling Radar (CPR), which operates at 94 GHz. The CPR was developed to provide vertical cloud structure information on different-sized particles that could not be determined using conventional passive sensors. CloudSat is also part of the satellite constellation of passive and active sensors called the A-Train [*Stephens et al.*, 2002]. Observations by A-Train sensors have been used to analyze the relationships among cloud droplets, drizzle, and precipitation and have provided new insights into warm cloud microphysics and its link to aerosols. Among recent studies using these data, *Lebsock et al.* [2008] reported aerosol effects on CloudSat radar reflectivity (Z_e), the liquid water path (LWP), and r_e over global oceans. *Suzuki and Stephens* [2008] found sixth-power and cubic relationships between Z_e and the effective particle radius of oceanic clouds, illustrating that condensation and coagulation constituted the dominant particle growth processes at smaller and larger Z_e values, respectively. *Kubar and Hartmann* [2008] collected data on tropical oceanic cloud vertical structures and quantified the relationship between cloud top height and precipitation rate. Most of

[1]Graduate School of Fisheries Science and Environmental Studies, Nagasaki University, Nagasaki, Japan.
[2]Department of Atmospheric Science, Colorado State University, Fort Collins, Colorado, USA.
[3]Now at Jet Propulsion Laboratory, California Institute of Technology, Pasadena, California, USA.

0148-0227/12/2011JD016412

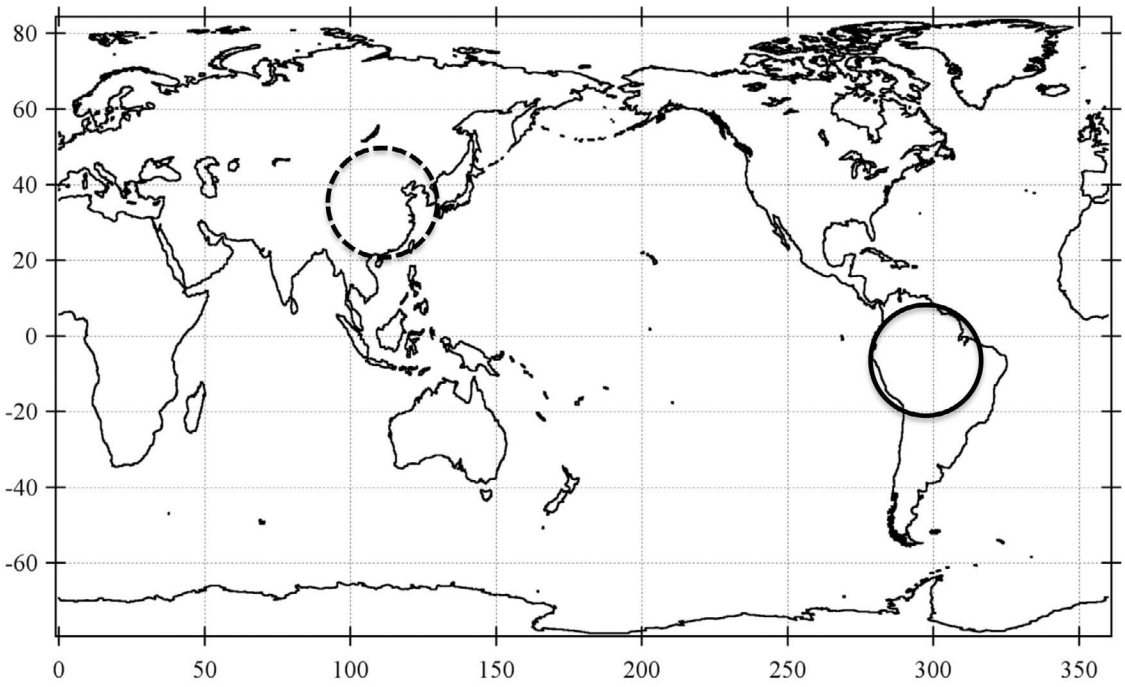

Figure 1. Map of the regions analyzed. The solid and dotted circles represent the Amazon (within 1500 km of 7°S and 60°W) and China (within 1800 km of 35°N and 120°E), respectively.

these previous studies, however, have been limited to oceanic clouds, partly due to their more uniform surface and the availability of microwave retrievals.

[5] On the other hand, *Kawamoto* [2008] compared the precipitation rate (P) obtained from ground-based measurements and microphysical properties of nonprecipitating water clouds derived from passive satellite sensor data over the Amazon and China, motivated by an earlier analysis of clouds over the Amazon [*Kawamoto*, 2006]. He reported a positive correlation between P and r_e and a negative correlation between P and columnar cloud particle number concentration as a unilateral effect of precipitation on nonprecipitating clouds, suggesting that precipitation was a factor that modifies the microphysical behaviors of nonprecipitating clouds [*Kawamoto*, 2008]. Although this idea is consistent with *Twomey*'s [1977] view of aerosol scavenging by precipitation as an external forcing, it is also important to investigate the mutual relationships between cloud and precipitation.

[6] In this study, we use the novel in-cloud information provided by CloudSat to describe the transitional processes and relationships among cloud droplets, drizzle, and precipitation in water clouds instead of the unilateral effect of precipitation on water clouds. To this end, we investigate several aspects of the cloud-to-precipitation transitional processes and relationships among cloud droplets, drizzle, and precipitation inside water clouds over the Amazon, within 1500 km of 7°S and 60°W, and over China, within 1800 km of 35°N and 120°E as indicated by the solid and dotted circles, respectively, in Figure 1. These regions were chosen because they have different latitudes and climatic regimes that would result in different precipitation types characterized by strong convection and frontal systems.

[7] This study is organized as follows. In section 2, we briefly describe the data sets used and the target clouds. Next, section 3 presents the main analyses of the occurrence frequencies of the cloud droplet number concentration (N_c) and Z_e, the fractional occurrences of different Z_e categories as a function of LWP, the behaviors of several cloud parameters among different Z_e categories, and the changes in cloud vertical structures according to N_c. Finally, section 4 summarizes the conclusions of this study.

2. Data Sets

[8] We use CloudSat data collocated with MODIS products for the periods of June, July, and August (JJA) and December, January, and February (DJF) during CloudSat operation from 2006 to 2010. The following data sets are used in this study: 2B-GEOPROF for the vertical distribution of Z_e and cloud mask [*Mace et al.*, 2007; *Marchand et al.*, 2008]; 2B-TAU for visible τ_c of the whole cloud layer, and r_e (with 2.15 μm band) at the cloud top derived from MODIS-observed radiances [*Polonsky*, 2008] (available from http://www.cloudsat.cira.colostate.edu/ICD/2B-TAU/tau2b_icd_v1.pdf); and ECMWF-AUX for altitude and temperature profiles from the European Center for Medium-Range Weather Forecasts (ECMWF) objective archives [*Partain*, 2007] (available from http://www.cloudsat.cira.colostate.edu/dataICDlist.php?go=list&path=/ECMWF-AUX]).

[9] We select only single-layered and water (liquid-phase) clouds having $\tau_c > 1$ and $r_e < 35$ (μm) to reduce the retrieval uncertainty of the above products. The former (single-layered) requirement is determined as follows according to the method of *Haynes and Stephens* [2007]. First, moving upward from the lowest layer, we examine whether layers

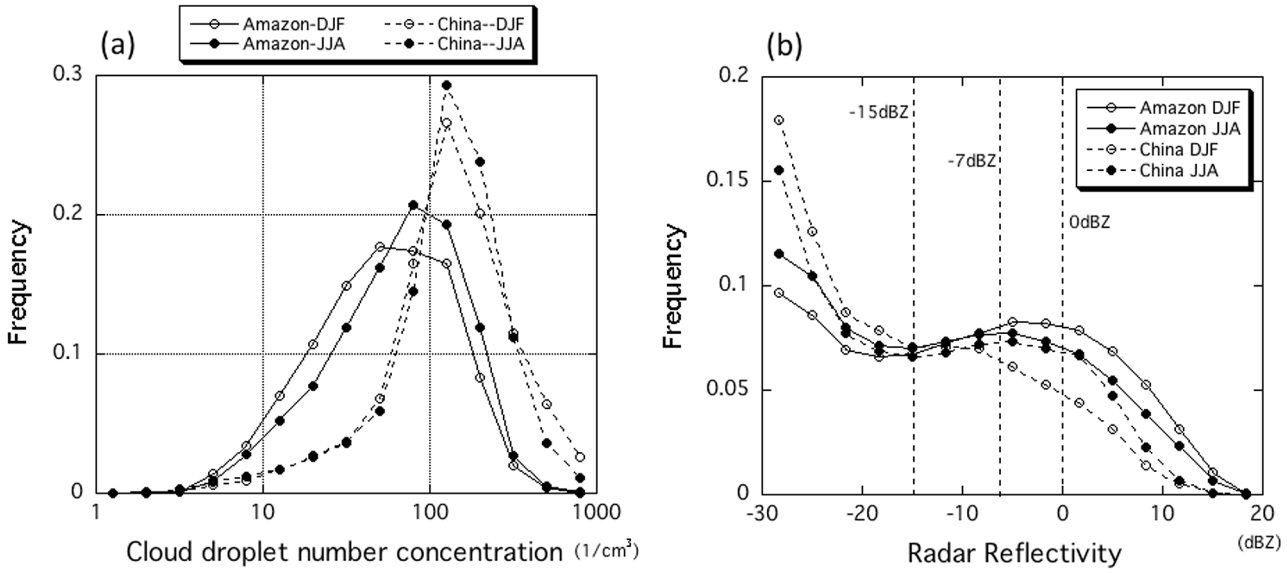

Figure 2. Frequency distributions of (a) N_c and (b) Z_e for all of the cloud layers over the Amazon and China for DJF and JJA. The three threshold values of −15, −7, and 0 (dBZ) are superimposed in Figure 2b.

meet the following three conditions: (1) the cloud mask value is between 30 and 40, (2) Z_e does not equal the undefined value, and (3) the height value is positive. The first height bin that satisfies all the conditions is considered the cloud base. Next, we examine the layers upward from the cloud base thus determined and identify the bins that satisfy all the conditions as the cloud layer. The layer just under the first layer not satisfying these conditions is defined as the "cloud top of the lower layer" (CTL). The same procedure is then conducted downward from the highest layer, and the first layer that satisfies all the conditions is termed the "cloud top of the higher layer" (CTH). If CTL and CTH are identical, we consider the cloud layer to be single layered. Otherwise, we conclude that the atmospheric column consists of multilayered clouds. The latter (liquid-phase) requirement is identified by the CloudSat cloud mask criterion and the echo-top temperature warmer than 273 K.

[10] We obtain 10,157 samples for Amazon-DJF, 11,075 for Amazon-JJA, 3,919 for China-DJF, and 10,645 for China-JJA. China-DJF has a much smaller sample size because fewer water clouds are present during the midlatitude winter.

3. Results

3.1. Occurrence Frequencies of N_c and Z_e

[11] Figure 2a shows the frequency distributions of N_c over the Amazon and China. Values for N_c are calculated based on the adiabatic growth model [e.g., *Brenguier et al.*, 2000] using equation (3) for N_{eff} of *Kubar et al.* [2009]:

$$N_c = \sqrt{2}B^3\Gamma_{\mathrm{eff}}{}^{1/2}\mathrm{LWP}^{1/2}/r_e^3, \qquad (1)$$

where $B = (3\pi\rho_w/4)^{1/3} = 0.0620$ and ρ_w is the density of liquid water. Γ_{eff} is the adiabatic rate of increase in the liquid water content with height, which is weakly dependent on pressure and temperature, and is taken from a diagram of *Wood* [2006] (available from http://www.atmos.washington.edu/∼robwood/papers/chilean_plume/optical_depth_relations.pdf) (for details, see *Kubar et al.* [2009, and references therein]). LWP is derived from MODIS products by $5\tau_c r_e/9$ assuming an adiabatic cloud process [e.g., *Brenguier et al.*, 2000].

[12] Generally, N_c over the Amazon is found to be lower than over China. The mode values are approximately 80 cm^{-3} and 150 cm^{-3} over the Amazon and China, respectively, which are reasonable for continental clouds judged from the results of aircraft measurements [e.g., *Squires*, 1958; *Gultepe and Isaac*, 2004]. Comparing different seasons, the N_c for Amazon-JJA is higher than that for Amazon-DJF. Over China, although the peak values of N_c are almost the same for DJF and JJA, the frequency for China-DJF is higher for larger values (>500 cm^{-3}). These regional and seasonal differences in N_c may reflect the signature of aerosol abundance, as supported by the MODIS-retrieved aerosol optical depth (AOD) values [*Remer et al.*, 2005], which are estimated as 0.12 and 0.11 for DJF and JJA, respectively, in the Amazon (characterized by biomass burning) and as 0.38 and 0.61 for DJF and JJA, respectively, in China (characterized by industrial and dust aerosols). These seasonal differences in N_c and AOD could be associated with the fact that DJF is the rainy season in the Amazon and the dry season in China, whereas JJA is the dry season in the Amazon and the rainy season in China. The seasonal variation in AOD may not correspond to that in N_c due to clear-sky bias of satellite data and incomplete matching of the observation period. Still, the characteristics of N_c found in Figure 2a can be interpreted to reflect such regional and seasonal differences in cloud condensation nuclei processes, including those involving emissions and wet scavenging due to precipitation.

[13] To investigate the drizzle and precipitation characteristics, Figure 2b shows the frequency distributions of Z_e

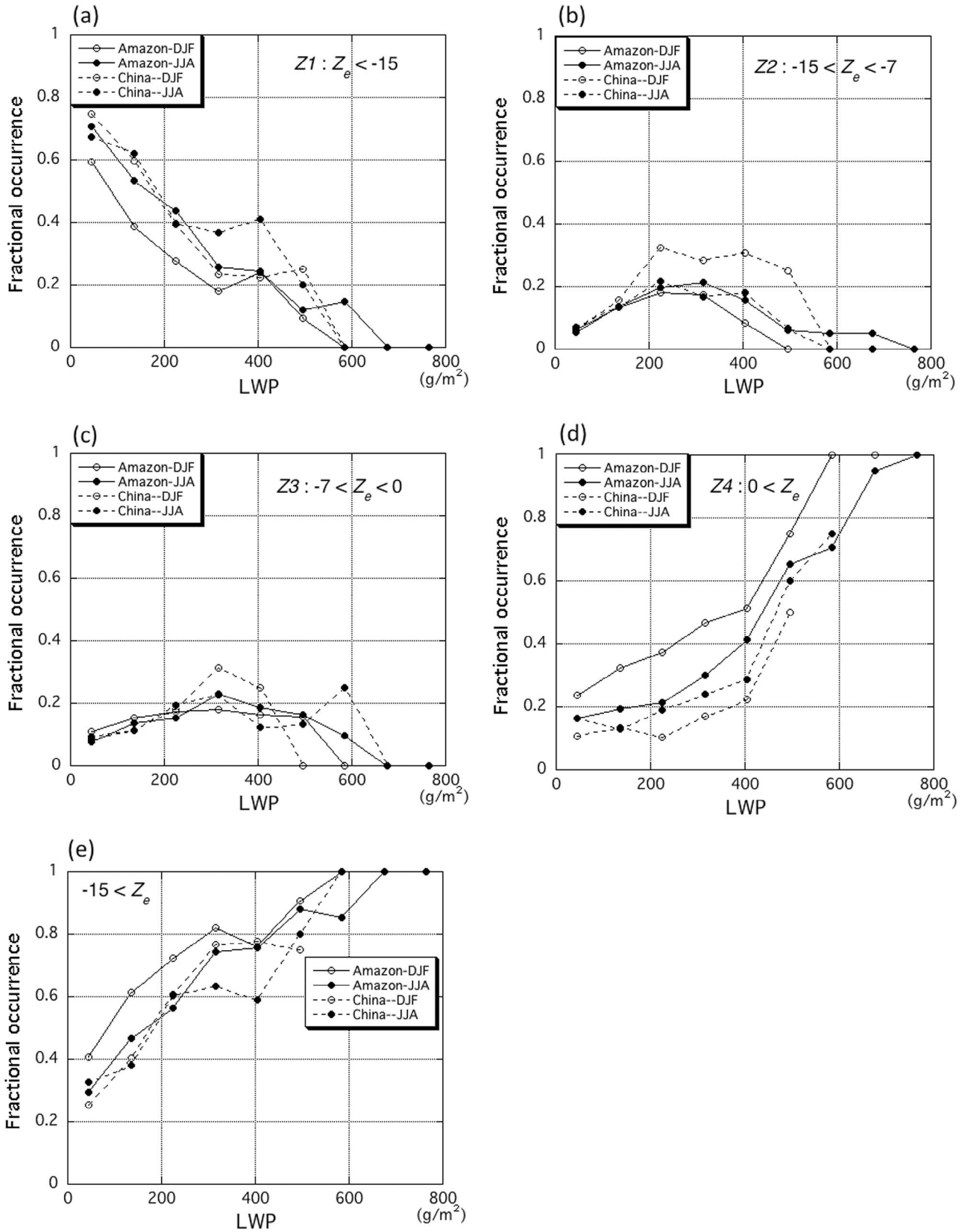

Figure 3. Fractional occurrences of the maximum Z_e for (a) nonprecipitating (Z_e1, $Z_e < -15$ dBZ), (b) drizzle (Z_e2, $-15 < Z_e < -7$ dBZ), (c) light precipitating (Z_e3, $-7 < Z_e < 0$ dBZ), (d) precipitating (Z_e4, 0 dBZ $< Z_e$), and (e) summation from Z_e2 to Z_e4 as a function of liquid water path (LWP) over the Amazon and China for DJF and JJA.

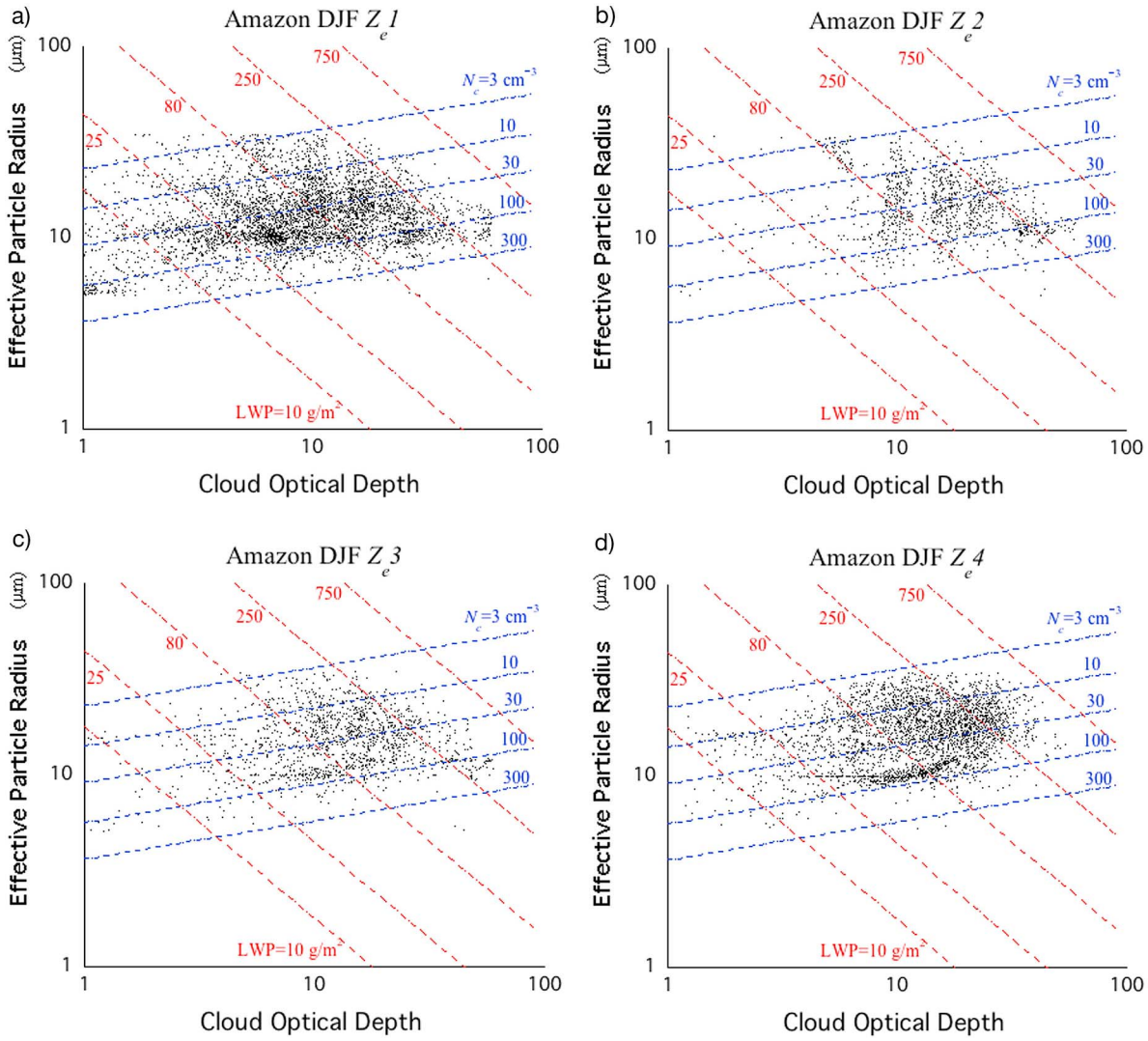

Figure 4. Scatterplots of τ_c and r_e with the theoretical relationships from the adiabatic cloud model under a constant N_c (for 3, 10, 30, 100, and 300 cm^{-3}) and LWP (for 10, 25, 80, 250, and 750 g/m^2) in (a) Amazon-DJF for Z_e1 ($Z_e < -15$ dBZ), (b) Amazon-DJF for Z_e2 ($-15 < Z_e < -7$ dBZ), (c) Amazon-DJF for Z_e3 ($-7 < Z_e < 0$ dBZ), (d) Amazon-DJF for Z_e4 (0 dBZ $< Z_e$), (e) China-DJF for Z_e1, (f) China-DJF for Z_e2, (g) China-DJF for Z_e3, and (h) China-DJF for Z_e4.

for all the cloud layers over the Amazon and China. Four precipitation categories are defined according to the Z_e value, as proposed by *L'Ecuyer et al.* [2009]: (1) non-precipitating ($Z_e < -15$ dBZ); (2) drizzle approximately corresponding to a rain rate of less than 0.01 mm/h (-15 dBZ $< Z_e < -7$ dBZ); (3) light precipitating corresponding to a rain rate of about 0.01∼0.03 mm/h (-7 dBZ $< Z_e < 0$ dBZ); and (4) precipitating (0 dBZ $< Z_e$). These four categories are hereafter referred to as Z_e1, Z_e2, Z_e3, and Z_e4, respectively, and three threshold values, -15 dBZ, -7 dBZ, and 0 dBZ are superimposed using dotted lines in Figure 2b. Figure 2b shows that the Z_e1 frequency in the Amazon in JJA (the dry season) is larger than that in DJF (the rainy season), whereas the Z_e4 frequency is higher in DJF than in JJA, as expected from the seasonality of precipitation. Although the differences in frequency between Z_e2 and Z_e3 are smaller than those between Z_e1 and Z_e4, we observe higher frequencies for Z_e3 in DJF. The trends in China are similar to those in the Amazon in seasonality (reversed in month). Moreover, the frequencies are higher for Z_e3 and Z_e4 in the rainy season (JJA in China). Comparing the Amazon and China groups, the Z_e1 frequencies are larger for China, with higher frequencies of about 10 dBZ in the larger Z_e4, implying a lower chance of no precipitation and more frequent precipitation in the Amazon. *Leon et al.* [2008] obtain similar bimodal features for the Z_e frequency in marine boundary layer clouds, consistent with our results.

3.2. Fractional Occurrence of Z_e Versus LWP

[14] Next, we analyze the fractional occurrence of the maximum Z_e within the cloud layer for the four categories (Z_e1–Z_e4) as a function of LWP, following the analysis method proposed by *Lebsock et al.* [2008] and *L'Ecuyer et al.*

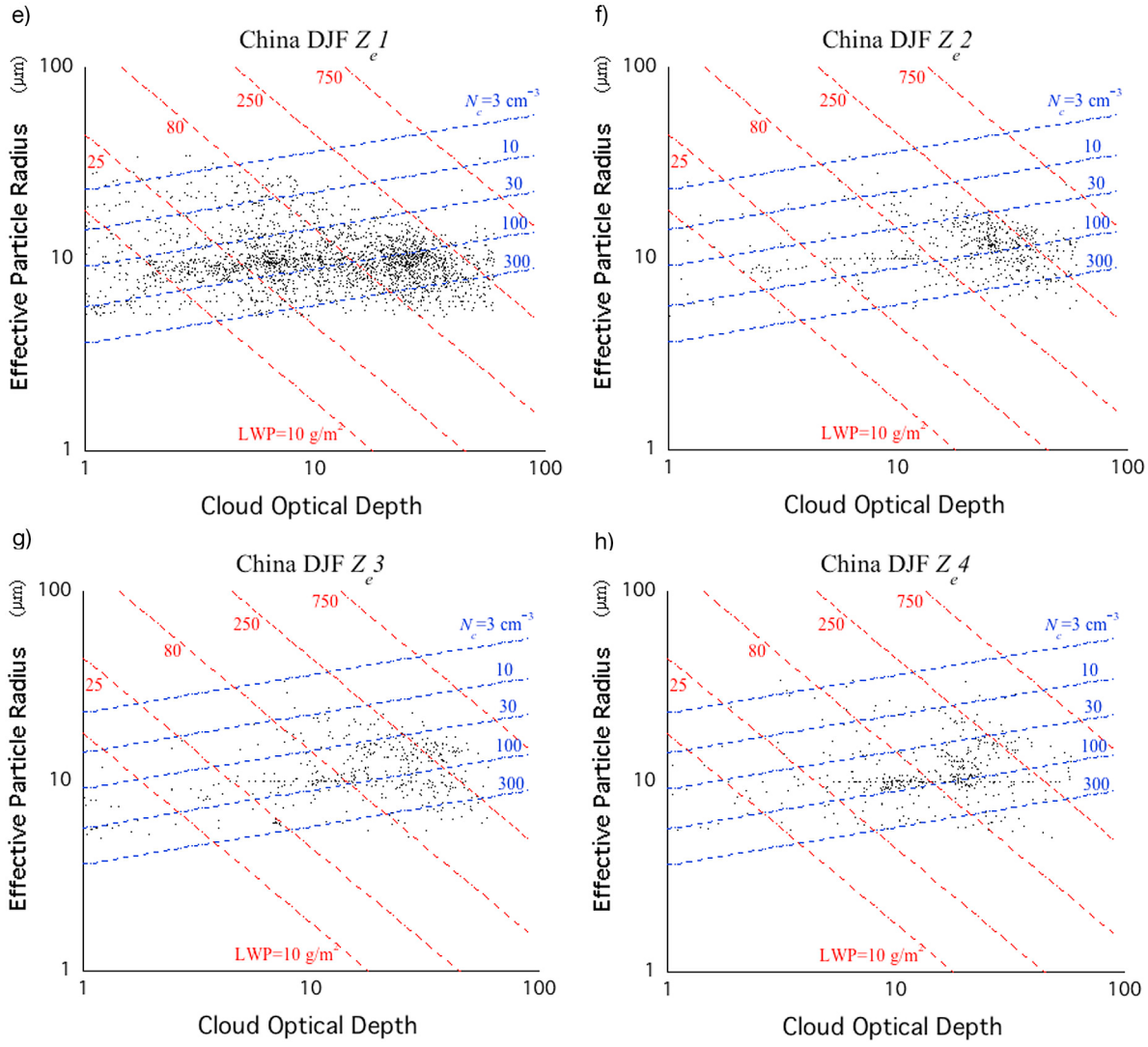

Figure 4. (continued)

[2009], who introduced the probability of precipitation (POP) and examined its relation to LWP. They found that POP tended to increase monotonically with LWP and was significantly modified by aerosol abundance, demonstrating how cloud water tended to be converted to rainwater and how aerosols tended to influence this conversion process. Although both *Lebsock et al.* [2008] and *L'Ecuyer et al.* [2009] used LWP from microwave remote sensing in their oceanic cloud studies, we use LWP values derived from MODIS τ_c and r_e because LWP retrieval using microwaves is impossible over land due to the difficulty in correcting bidirectionality. According to *Horváth and Davies* [2007], who compared LWP values from microwave (Tropical Rainfall Measuring Mission Microwave Imager (TMI)) and optical (MODIS and Multiangle Imaging Spectroradiometer (MISR)) estimates, both values are in quite good agreement, with an overall correlation coefficient of 0.85 and RMS difference of 25 g/m^2 for LWP < 300 g/m^2. Larger LWP values than this threshold seem to be more uncertain, although this was not quantified by *Horváth and Davies* [2007].

[15] Figure 3 shows the results of this analysis. Note that these panels do not show the probability distribution function (PDF) as in Figures 2a and 2b, but show fractional occurrences. In Figure 3a, an almost monotonic decline in

Table 1. Average and Standard Deviation Values of the Warm Cloud Parameters for the Four Z_e Categories Over the Amazon and China (DJF)[a]

	τ_c	r_e (μm)	N_c (cm^{-3})	LWP (g/m^2)
Amazon Z_e1	11.8 (15.4)	13.7 (14.7)	88.6 (119.2)	89.7 (117.1)
Amazon Z_e2	18.3 (21.5)	16.0 (17.1)	85.5 (124.2)	152.1 (173.1)
Amazon Z_e3	15.7 (19.1)	15.8 (16.8)	75.4 (108.6)	135.3 (162.9)
Amazon Z_e4	14.3 (16.4)	17.3 (18.3)	56.9 (76.9)	143.3 (175.0)
China Z_e1	15.9 (20.5)	10.3 (11.0)	196.5 (265.8)	86.4 (111.8)
China Z_e2	24.7 (28.2)	11.7 (12.2)	168.9 (221.9)	157.8 (180.7)
China Z_e3	21.1 (25.0)	11.6 (12.3)	170.3 (232.7)	139.3 (168.9)
China Z_e4	17.4 (20.6)	11.9 (12.8)	155.9 (221.2)	116.1 (145.3)

[a]Standard deviations are in parentheses. LWP, liquid water path.

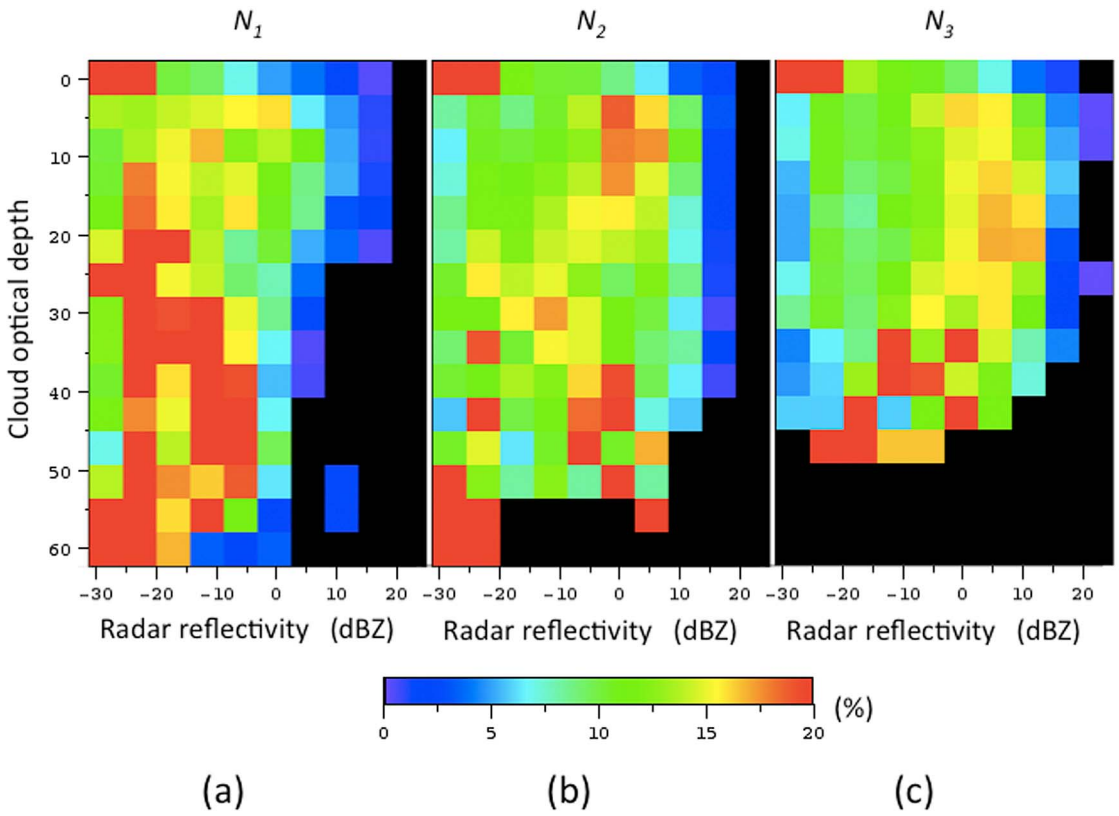

Figure 5. Contoured frequency by optical depth diagram of the (a) Amazon-DJF for N_1 (100 cm^{-3} < N_c), (b) Amazon-DJF for N_2 (40 cm^{-3} < N_c < 100 cm^{-3}), (c) Amazon-DJF for N_3 (N_c < 40 cm^{-3}), (d) Amazon-JJA for N_1, (e) Amazon-JJA for N_2, (f) Amazon-JJA for N_3, (g) China-DJF for N_1, (h) China-DJF for N_2, (i) China-DJF for N_3, (j) China-JJA for N_1, (k) China-JJA for N_2, and (l) China-JJA for N_3.

the Z_e1 category is shown with increasing LWP, indicating a greater chance of no precipitation at smaller LWP values. It is reasonable that the lowest occurrence for the nonprecipitating category is found for Amazon-DJF, when precipitation is most likely to occur among the four cases. In Figure 3b, most peaks in Z_e2 occurrence are found around LWP = 300 g/m^2. Notably, while the fractional occurrences of the Z_e3 category (Figure 3c) have a convex top similar to those of the Z_e2 category (Figure 3b), most occurrences are shifted to larger LWP values in Figure 3c, suggesting stronger precipitation in Z_e3 than Z_e2, as *L'Ecuyer et al.* [2009] also found for oceanic clouds. The dry season in China (DJF) has larger occurrences for less strong precipitation categories in both Figures 3b and 3c. Figure 3d shows the fractional occurrence of the Z_e4 category. In general, monotonic increases in POP with increasing LWP are observed, in contrast to Figure 3a. Moreover, Amazon-DJF, representing the rainy season, has larger occurrences than the other three cases throughout the LWP range, and the POP becomes 100% at around 600 g/m^2, whereas for China, the POP is less than 80%. These overall tendencies are quite similar to the results of *L'Ecuyer et al.* [2009]. As our method of calculating POP based on the maximum Z_e within the cloud layer differs from that of *L'Ecuyer et al.* [2009], who used attenuation-corrected near surface reflectivity, these two analyses cannot be compared quantitatively. Finally, Figure 3e shows the summed fractional occurrences of Z_e2, Z_e3, and Z_e4 (i.e., drizzle, light precipitating, and precipitating, but not nonprecipitating) as a function of LWP. Hereafter, we call this occurrence the drizzle frequency, following *Kubar et al.* [2009]. Most curves show the monotonic increase and asymptotic approach to unity at around 600 g/m^2, except the China-DJF case (dry season), which approaches 0.8 asymptotically at a smaller LWP of about 300 g/m^2. *Kubar et al.* [2009] examined a similar analysis for oceanic clouds and found a strong increase in the drizzle frequency with LWP, although for a given LWP, drizzle was more frequent in pristine regions. It is important to note that in their study, the drizzle frequency approached 100% at around 400 g/m^2 in the more pristine regions [see *Kubar et al.*, 2009, Figure 11b]; in our study, the LWPs required for a nearly 100% drizzle frequency are considerably higher. This is consistent with the behavior in the more polluted regions such as the Asian coast and Gulf of Mexico in their study. *Zuidema et al.* [2005] examined drizzle occurrence as a function of LWP over the southeast Pacific, and their results support the above relationship. As *Zuidema et al.* [2005] and *Kubar et al.* [2009] examined oceanic clouds whose LWP covered somewhat narrower ranges than those in this study, it would be beneficial to revisit these studies to understand the difference in the development properties of clouds over ocean and land.

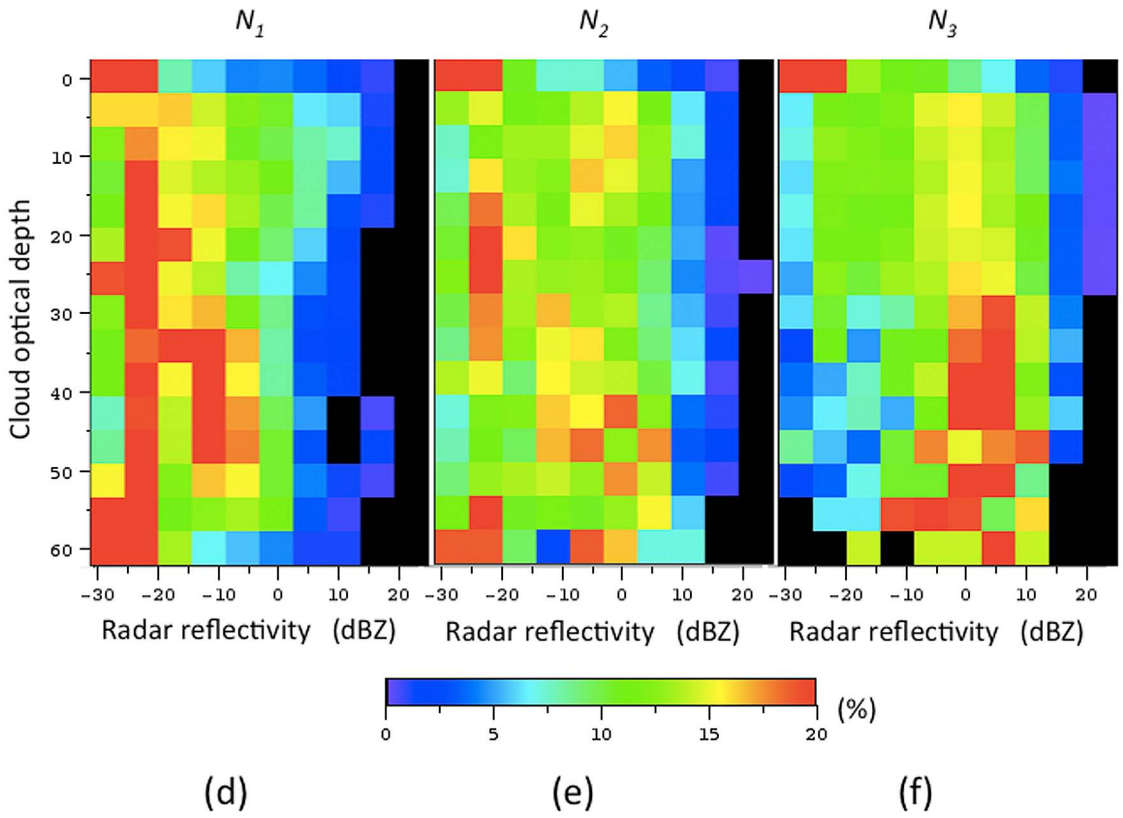

Figure 5. (continued)

3.3. Behaviors of Cloud Parameters Among Z_e Categories

[16] *Suzuki et al.* [2010a, 2010b] proposed that the correlation statistics between τ_c and r_e contained a signature of droplet growth processes, including condensation, coalescence, and evaporation [see *Suzuki et al.*, 2010a, Figure 7] based on a spectral bin microphysics modeling study aimed at interpreting correlation statistics reported by remote sensing studies [e.g., *Nakajima et al.*, 1991; *Nakajima and Nakajima*, 1995].

[17] These studies found positive and negative correlations between τ_c and r_e. The correlation patterns were proposed to include the physical background as follows. A positive correlation reflects the following: (1) r_e becomes larger in the growth stage, and τ_c gets larger via an increase in LWP and (2) r_e becomes smaller due to evaporation, and this loss of cloud water results in a decrease in τ_c. Conversely, a negative correlation reflects the following: (1) r_e becomes larger through mainly the coalescence process, and the subsequent precipitation reduces τ_c via the loss of cloud water and (2) r_e becomes smaller in an aerosol rich environment, and the enhanced total cross section of cloud droplets causes an increase in τ_c when the amount of cloud water is fixed.

[18] Here, we investigate the behaviors of cloud parameters (τ_c, r_e, N_c, and LWP) over the Amazon and China for different Z_e categories to examine how they tend to relate to the different precipitation categories. As we have confirmed that the seasonal change was similar in DJF and JJA, only the DJF case is presented here. Figure 4 shows the scatterplots of τ_c and r_e for the four Z_e categories, along with the theoretical relationships from the adiabatic cloud model under a constant N_c and LWP: Amazon-DJF Z_e1–Z_e4 (Figures 4a–4d) and China-DJF Z_e1–Z_e4 (Figures 4e–4h). The lines for specified values of N_c and LWP apply to the growth condition via the condensation process and the vertical extent of the cloud layer, respectively [*Suzuki et al.*, 2010a, 2010b]. Although it is difficult to identify distinct positive or negative correlation patterns in Figure 4, unlike the analyses by *Nakajima and Nakajima* [1995] and *Suzuki et al.* [2010a, 2010b], we will discuss the transitional tendencies among Z_e1–Z_e4 for both regions, together with the average and standard deviation of τ_c, r_e, N_c, and LWP listed in Table 1. First, the average τ_c is the smallest for Z_e1 and largest for Z_e2, and it then decreases from Z_e3 to Z_e4 for both regions, as LWP shows similar tendencies despite the large standard deviation. For this phenomenon, we hypothesize that clouds start to store water or decay via evaporation in Z_e1; thus, they store the maximum amount of water in Z_e2 at the onset of drizzle and then start to precipitate, decreasing cloud water gradually from Z_e3 to Z_e4. As for r_e, continuous increases from Z_e1 to Z_e4 are recognized for both the Amazon and China due to the greatest chance of precipitation during Z_e4, regardless of the similar r_e values for Z_e2 and Z_e3. The opposite tendency to r_e is observed for N_c. *Kubar*

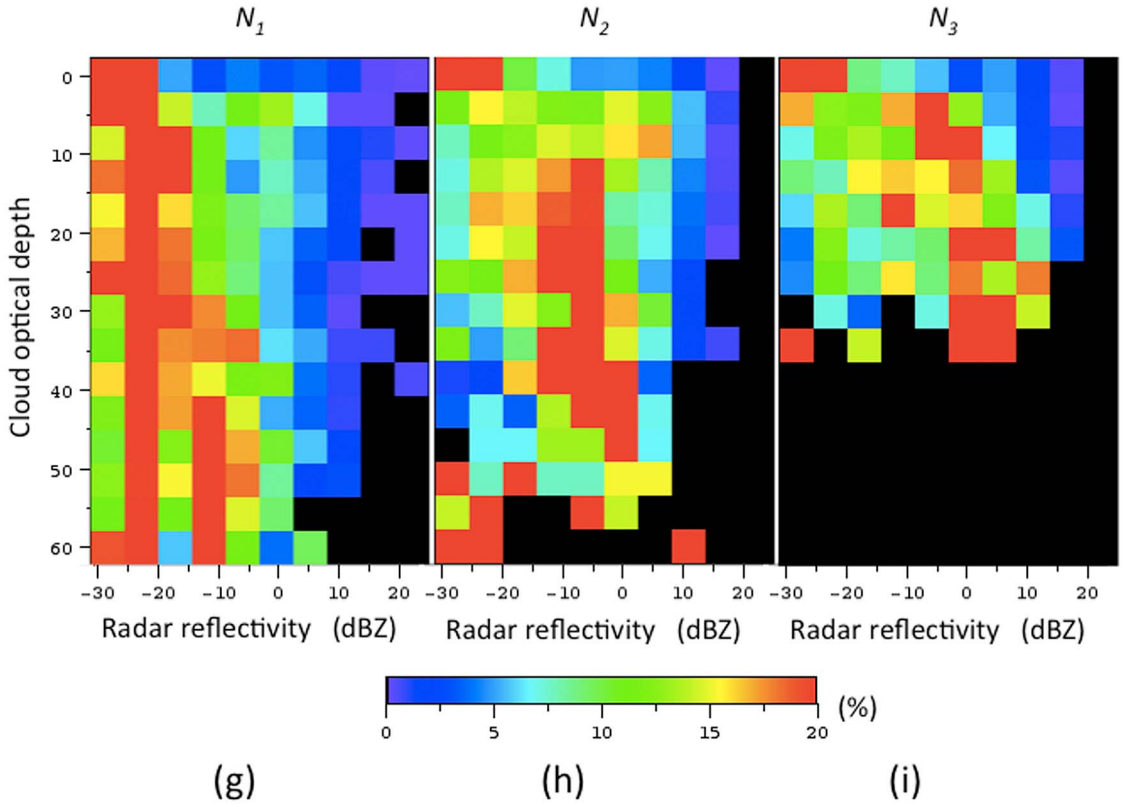

Figure 5. (continued)

et al. [2009] plotted the median LWP, r_e, and N_c as a function of the median maximum Z_e [see *Kubar et al.*, 2009, Figures 9b, 10a, and 10b]. Although the tendencies for the behavior of r_e and N_c versus the Z_e categories are the same in our and their analyses, the tendency with respect to LWP behavior in our analysis differs from that of *Kubar et al.* [2009], who reported a monotonic increase in LWP. It is interesting to consider what causes this difference in view of the land–ocean contrast. We also find that the absolute values of τ_c are larger over China than over the Amazon, whereas those of r_e are larger over the Amazon than over China, consistent with the discussion of Figure 3a) and the aerosol indirect effect of the first kind [*Twomey*, 1977]. Additionally, the range of variation of r_e is obviously smaller for China (more flattened patterns are found in Figures 4e–4h), reflecting more AOD caused by active emission and less intensive precipitation.

3.4. Vertical Cloud Structure

[19] The unique vertical profile capability of CloudSat, when combined with MODIS shortwave analysis, provides new insight into microphysical processes occurring inside the cloud layer, as recently illustrated by *Nakajima et al.* [2010] and *Suzuki et al.* [2010c]. These studies proposed the use of optical depth (as the y axis), instead of geometric height, to analyze Z_e profiles (as the x axis) by constructing a new diagram called the contoured frequency by optical depth diagram (CFODD), in which Z_e profiles are rescaled as a function of in-cloud optical depth determined from the MODIS-derived τ_c. However, *Nakajima et al.* [2010] adopted the in-cloud optical depth determined by the vertical profiles of Z_e, which made the x and y axes not completely independent. To solve this problem, *Suzuki et al.* [2010c] introduced an adiabatic growth model to obtain the in-cloud optical depth and found that the vertical microphysical structures in these diagrams clearly transitioned from cloud through drizzle to precipitation as a fairly monotonic function of the MODIS-derived r_e.

[20] We use the CFODD approach to investigate the vertical structures of warm clouds over the Amazon and China. Although *Nakajima et al.* [2010] and *Suzuki et al.* [2010c] classified CFODDs according to r_e, we classify CFODDs according to N_c to more directly interpret the cloud parameter relationship to the aerosol effect. This approach helps reveal how the vertical particle growth patterns relate to N_c. For this purpose, three N_c categories, referred to as N_1, N_2, and N_3, corresponding to higher, moderate, and lower cloud droplet number populations, respectively, are defined with thresholds of 40 cm^{-3} and 100 cm^{-3}. Figure 5 shows the CFODDs constructed separately for the N_1–N_3 cases for Amazon-DJF (Figures 5a–5c), Amazon-JJA (Figures 5d–5f), China-DJF (Figures 5g–5h), and China-JJA (Figures 5j–5l).

[21] In most cases, the high-frequency parts shift to a larger Z_e and smaller τ_c, as N_c decreases from N_1 to N_3. We interpret this phenomenon as follows. After the developing stage, N_c decreases and r_e increases through coalescence, which results in decreasing τ_c due to the reduction in the total cross section of particles. Moreover, the total water amount inside clouds decreases by precipitation. Evaporation can also decrease the particle size and further eliminate

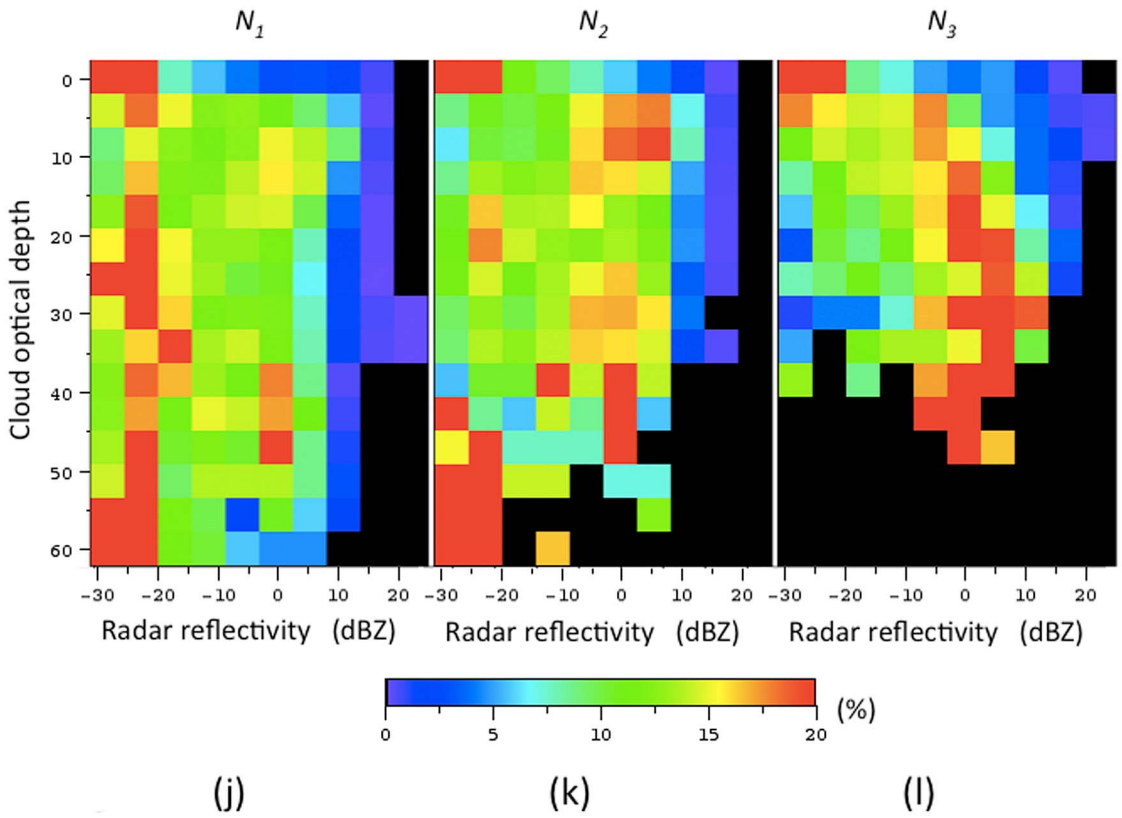

Figure 5. (continued)

particles themselves, both of which result in decreasing τ_c by losing the liquid water as shown in Figure 4.

[22] N_3 has a high frequency for larger Z_e, suggesting a higher occurrence of precipitation, whereas N_1 has a high frequency for smaller Z_e, denoting little precipitation. This suggests that N_2 is a transitional state between N_1 and N_3. Furthermore, the vertical extension is larger in the Amazon because of stronger convection around the tropics, especially in the N_3 cases. In China, precipitation occurs with optically thinner clouds than in the Amazon, as illustrated in Figures 5i and 5l.

4. Conclusions

[23] As a natural extension of the research of *Kawamoto* [2008], who interpreted correlation statistics between the precipitation rate and nonprecipitating water cloud microphysics as the unilateral effect of precipitation via aerosol scavenging, this study describes and compares the transitional processes and relationships among cloud droplets, drizzle, and precipitation in single-layer water clouds over the Amazon and China, regions characterized by different climatic conditions at different latitudes, as indicated in Figure 1.

[24] We apply several analysis methods based on the synergistic use of products from the active CloudSat and passive MODIS sensors. In Figure 2, the difference in N_c found over the two regions in DJF and JJA indicates the regional and seasonal differences in aerosol abundance, with N_c generally lower over the Amazon and higher over China. Additionally, the seasonal variation in N_c is consistent with precipitation scavenging caused by the rainy/dry seasonal contrast. The Z_e frequencies are also consistent with the annual cycle of the precipitation rate between the rainy (DJF for the Amazon and JJA for China) and dry (JJA for the Amazon and DJF for China) seasons over these two regions.

[25] Furthermore, as shown in Figure 3, the fractional occurrence of the Z_e categories as a function of LWP shows an almost monotonic decline and increase for Z_e1 (nonprecipitating) and Z_e4 (precipitating) occurrences, respectively. It is also reasonable that Amazon-DJF, which has the highest precipitation probability, shows the lowest and highest probabilities in Z_e1 and Z_e4, respectively. Although the shapes of fractional occurrence are similar for the Z_e2 and Z_e3 cases, it is interesting that the Z_e3 case (light precipitating) has peaks at larger LWP compared with the Z_e2 case (drizzle), and that China-DJF, which has the lowest precipitation probability, has the highest values in both the Z_e2 and Z_e3 cases. Moreover, the drizzle frequency, defined as the summed fractional occurrence of Z_e2, Z_e3, and Z_e4 as a function of LWP, shows a similar tendency to the result of *Kubar et al.* [2009], who analyzed oceanic clouds, but the difference in LWP values for 100% precipitation occurrence would be of interest to understand the differences in developmental stages of clouds over ocean and land.

[26] The behaviors of the cloud parameters among different Z_e categories reveal regional differences in microphysical variation; for example, the absolute value and the variation range of r_e are smaller over China as shown in Figure 4. Above all, using independent methods, it would be

worthwhile to verify the hypothesis that clouds start to store water or decay through evaporation in Z_e1; thus, they store the maximum amount of water in Z_e2 at the onset of drizzle and then start to precipitate, decreasing cloud water gradually from Z_e3 to Z_e4, although more robust statistical analyses are needed.

[27] Finally, using CFODDs, the cloud vertical characteristics are methodically compared between the regions and the seasons as a function of N_c in Figure 5. This approach illustrates that water clouds become optically thinner and produce precipitation (shifting to larger Z_e) through the coalescence of droplets as N_c decreases. In this case, the evaporation process would also play an important role in reducing τ_c. Regional differences between the Amazon and China in cloud vertical development can be attributed to differences in convection strength and in precipitation that occurred in optically thicker parts over the Amazon than over China. These characteristics would be closely connected to combinations of differences in dynamical and particle environments between low-latitude convective and midlatitude frontal zones. Finally, we note that synergistic use of multiple observation products and numerical modeling can aid in exploring the mechanisms of phenomena that include various development stages.

[28] **Acknowledgments.** K. Kawamoto was supported by the Mitsui and Co., Ltd., Environment Fund and by a Grant-in-Aid for Scientific Research on Innovative Areas. The CloudSat data products of 2B-GEOPROF, MODIS-AUX, and ECMWF-AUX were provided by the CloudSat Data Processing Center at CIRA/Colorado State University. The comments and suggestions of three anonymous reviewers greatly enhanced the quality of this paper.

References

Brenguier, J., H. Pawlowska, L. Schuller, R. Preusker, J. Fischer, and Y. Fouquart (2000), Radiative properties of boundary layer clouds: Droplet effective radius versus number concentration, *J. Atmos. Sci.*, *57*, 803–821, doi:10.1175/1520-0469(2000)057<0803:RPOBLC>2.0.CO;2.

Gultepe, I., and G. A. Isaac (2004), Aircraft observations of cloud droplet number concentration: Implications for climate studies, *Q. J. R. Meteorol. Soc.*, *130*, 2377–2390, doi:10.1256/qj.03.120.

Han, Q., W. B. Rossow, and A. A. Lacis (1994), Near-global survey of effective droplet radii in liquid water clouds using ISCCP data, *J. Clim.*, *7*, 465–497, doi:10.1175/1520-0442(1994)007<0465:NGSOED>2.0.CO;2.

Haynes, J. M., and G. L. Stephens (2007), Tropical oceanic cloudiness and the incidence of precipitation: Early results from CloudSat, *Geophys. Res. Lett.*, *34*, L09811, doi:10.1029/2007GL029335.

Horváth, A., and R. Davies (2007), Comparison of microwave and optical cloud water path estimates from TMI, MODIS, and MISR, *J. Geophys. Res.*, *112*, D01202, doi:10.1029/2006JD007101.

Kawamoto, K. (2006), Relationships between cloud properties and precipitation amount over the Amazon basin, *Atmos. Res.*, *82*, 239–247, doi:10.1016/j.atmosres.2005.10.007.

Kawamoto, K. (2008), Effect of precipitation on water cloud properties over China, *Geophys. Res. Lett.*, *35*, L20811, doi:10.1029/2008GL035052.

Kawamoto, K., T. Nakajima, and T. Y. Nakajima (2001), A global determination of cloud microphysics with AVHRR remote sensing, *J. Clim.*, *14*, 2054–2068, doi:10.1175/1520-0442(2001)014<2054:AGDOCM>2.0.CO;2.

Kubar, T. L., and D. L. Hartmann (2008), Vertical structure of tropical oceanic convective clouds and its relation to precipitation, *Geophys. Res. Lett.*, *35*, L03804, doi:10.1029/2007GL032811.

Kubar, T. L., D. L. Hartmann, and R. Wood (2009), Understanding the importance of microphysics and macrophysics for warm rain in marine low clouds. Part I: Satellite observations, *J. Atmos. Sci.*, *66*, 2953–2972, doi:10.1175/2009JAS3071.1.

Lebsock, M. D., G. L. Stephens, and C. Kummerow (2008), Multisensor satellite observations of aerosol effects on warm clouds, *J. Geophys. Res.*, *113*, D15205, doi:10.1029/2008JD009876.

L'Ecuyer, T. S., W. Berg, J. Haynes, M. Lebsock, and T. Takemura (2009), Global observations of aerosol impacts on precipitation occurrence in warm maritime clouds, *J. Geophys. Res.*, *114*, D09211, doi:10.1029/2008JD011273.

Leon, D. C., Z. Wang, and D. Liu (2008), Climatology of drizzle in marine boundary layer clouds based on 1 year of data from CloudSat and Cloud-Aerosol Lidar and Infrared Pathfinder Satellite Observations (CALIPSO), *J. Geophys. Res.*, *113*, D00A14, doi:10.1029/2008JD009835.

Mace, G. G., R. Marchand, Q. Zhang, and G. Stephens (2007), Global hydrometeor occurrence as observed by CloudSat: Initial observations from summer 2006, *Geophys. Res. Lett.*, *34*, L09808, doi:10.1029/2006GL029017.

Marchand, R., G. G. Mace, T. Ackerman, and G. Stephens (2008), Hydrometeor detection using CloudSat—An Earth-orbiting 94 GHz cloud radar, *J. Atmos. Oceanic Technol.*, *25*, 519–533, doi:10.1175/2007JTECHA1006.1.

Nakajima, T. Y., and T. Nakajima (1995), Wide-area determination of cloud microphysical properties from NOAA AVHRR measurements for FIRE and ASTEX regions, *J. Atmos. Sci.*, *52*, 4043–4059, doi:10.1175/1520-0469(1995)052<4043:WADOCM>2.0.CO;2.

Nakajima, T., M. D. King, J. D. Spinhirne, and L. F. Radke (1991), Determination of the optical thickness and effective particle radius of clouds from reflected solar radiation measurements. Part II: Marine stratocumulus observations, *J. Atmos. Sci.*, *48*, 728–751, doi:10.1175/1520-0469(1991)048<0728:DOTOTA>2.0.CO;2.

Nakajima, T. Y., K. Suzuki, and G. L. Stephens (2010), Droplet growth in warm water clouds observed by the A-Train. Part II: A multi-sensor view, *J. Atmos. Sci.*, *67*, 1897–1907, doi:10.1175/2010JAS3276.1.

Partain, P. (2007), Cloudsat ECMWF-AUX auxiliary data process description and interface control document, report, 10 pp., CloudSat Proj., Colo. State Univ., Fort Collins.

Platnick, S., M. D. King, S. A. Ackerman, W. P. Menzel, B. A. Baum, J. C. Riedi, and R. A. Frey (2003), The MODIS cloud products: Algorithms and examples from Terra, *IEEE Trans. Geosci. Remote Sens.*, *41*, 459–473, doi:10.1109/TGRS.2002.808301.

Polonsky, I. (2008), Level 2 cloud optical depth product process description and interface control document, report, 21 pp., CloudSat Proj., Colo. State Univ., Fort Collins.

Remer, L. A., et al. (2005), The MODIS aerosol algorithm, products and validation, *J. Atmos. Sci.*, *62*, 947–973, doi:10.1175/JAS3385.1.

Squires, P. (1958), The microstructure and colloidal stability of warm clouds. Part I: The relation between structure and stability, *Tellus*, *10*, 256–261, doi:10.1111/j.2153-3490.1958.tb02011.x.

Stephens, G. L., et al. (2002), The CloudSat mission and the A-Train, *Bull. Am. Meteorol. Soc.*, *83*, 1771–1790, doi:10.1175/BAMS-83-12-1771.

Stephens, G. L., et al. (2008), CloudSat mission: Performance and early science after the first year of operation, *J. Geophys. Res.*, *113*, D00A18, doi:10.1029/2008JD009982.

Suzuki, K., and G. L. Stephens (2008), Global identification of warm cloud microphysical processes with combined use of A-Train observations, *Geophys. Res. Lett.*, *35*, L08805, doi:10.1029/2008GL033590.

Suzuki, K., T. Nakajima, T. Y. Nakajima, and A. P. Khain (2010a), A study of microphysical mechanisms for correlation pattern between droplet radius and optical thickness of warm clouds with a spectral bin microphysics cloud model, *J. Atmos. Sci.*, *67*, 1126–1141, doi:10.1175/2009JAS3283.1.

Suzuki, K., T. Nakajima, T. Y. Nakajima, and G. L. Stephens (2010b), Effect of the droplet activation process on microphysical properties of warm clouds, *Environ. Res. Lett.*, *5*, 024012, doi:10.1088/1748-9326/5/2/024012.

Suzuki, K., T. Y. Nakajima, and G. L. Stephens (2010c), Particle growth and drop collection efficiency of warm clouds as inferred from joint CloudSat and MODIS observations, *J. Atmos. Sci.*, *67*, 3019–3032, doi:10.1175/2010JAS3463.1.

Twomey, S. (1977), The influence of pollution on the shortwave albedo of clouds, *J. Atmos. Sci.*, *34*, 1149–1152, doi:10.1175/1520-0469(1977)034<1149:TIOPOT>2.0.CO;2.

Wood, R. (2006), Relationships between optical depth, liquid water path, droplet concentration, and effective radius in adiabatic layer cloud, report, 3 pp., Univ. of Wash., Seattle.

Zuidema, P., E. R. Westwater, C. Fairall, and D. Hazen (2005), Ship-based liquid water path estimates in marine stratocumulus, *J. Geophys. Res.*, *110*, D20206, doi:10.1029/2005JD005833.

K. Kawamoto, Graduate School of Fisheries Science and Environmental Studies, Nagasaki University, 1-14 Bunkyo-machi, Nagasaki 852-8521, Japan. (kazukawa@nagasaki-u.ac.jp)

K. Suzuki, Jet Propulsion Laboratory, California Institute of Technology, 4800 Oak Grove Dr., MS 233-300, Pasadena, CA 91109, USA.